Res Chem Intermed (2016) 42:595–609
DOI 10.1007/s11164-015-2044-z

Sol–gel preparation and characterization of Ag and Mg co-doped nano TiO_2: efficient photocatalytic degradation of C.I. Acid Red 27

Jila Talat-Mehrabad[1] · Morteza Khosravi[1] · Nasser Modirshahla[2] · Mohammad A. Behnajady[2]

Received: 6 January 2015 / Accepted: 2 April 2015 / Published online: 14 April 2015

Abstract In this study, we successfully prepared pure, mono-doped, and Ag, Mg co-doped TiO_2 nanoparticles using the sol–gel method, with titanium tetraisopropoxide as the Ti source. The prepared samples were characterized by X-ray powder diffraction (XRD), specific surface area and porosity (BET and BJH) measurement, scanning electron microscopy, transmission electron microscopy, X-ray photoelectron spectroscopy, photoluminescence, and energy dispersive X-ray spectroscopy techniques. The XRD data showed that the prepared nanoparticles had the same crystals structures as the pure TiO_2. Also, DRS results indicated that the band gap of co-doped photocatalyst was smaller than that of the monometallic and undoped TiO_2 and that there was a shift in the absorption band towards the visible light region. Furthermore, the photocatalytic activity of the prepared catalysts was evaluated by the degradation of C.I. Acid Red 27 in aqueous solution under visible light irradiation. The results showed that Ag (0.08 mol%), Mg (0.2 mol%) co-doped TiO_2 had the highest photoactivity among all samples under visible light. It was concluded that co-doping of the Ag and Mg can significantly improve the photocatalytic activity of the prepared photocatalysts, due to the efficient inhibition of the recombination of photogenerated electron–hole pairs. The optimum calcination temperature and time were 450 °C and 3 h, respectively.

Keywords Heterogeneous photocatalysis · Co-doped TiO_2 · C.I. Acid Red 27 · Sol–gel method

✉ Morteza Khosravi
morteza.khosravi160@gmail.com; m_khosravi@iau-tnb.ac.ir

[1] Department of Applied Chemistry, North Tehran Branch, Islamic Azad University, Tehran, Iran

[2] Department of Chemistry, Tabriz Branch, Islamic Azad University, Tabriz, Iran

Introduction

Semiconductor mediated degradation of different organic pollutants has been widely investigated over the past few decades [1–3]. Among the various semiconductor materials employed, TiO_2 has been regarded as one of the most promising photocatalysts for degradation of organic pollutants, because of its high catalytic efficiency, high refractive index, thermal and electrical properties, resistance to photocorrosion, chemical stability, low cost and non-toxicity [4, 5]. When the energy (photon) supply is equal to or greater than that of the band gap energy, E_g of the photocatalyst, the excited electron in the valence band is transferred to the empty conduction band. This, in turn, leads to the generation of a positive hole (h^+_{vb})–electron (e^-_{cb}) pairs, according to (Eq. 1)

$$TiO_2 + h\nu \rightarrow e^-_{cb} + h^+_{vb} \quad (1)$$

In this reaction, the positive hole and electron are powerful oxidizing and reducing agents, respectively, according to (Eqs. 2, 3, 4)

$$h^+_{vb} + H_2O \rightarrow {}^{\cdot}OH + H^+ \quad (2)$$

$$h^+_{vb} + OH^- \rightarrow {}^{\cdot}OH \quad (3)$$

$$e^-_{cb} + O_2 \rightarrow {}^{\cdot -}O_2 \quad (4)$$

Thus, the organic pollutant is oxidized to form salts, carbon dioxide and water in the complete photocatalytic oxidation process [6], according to (Eq. 5)

$${}^{\cdot}OH + \text{pollutant} \rightarrow \text{products (salts, } CO_2, H_2O) \quad (5)$$

However, the low electron–hole separation rate of TiO_2 limits the efficiency of photocatalytic degradation of the pollutants. Also, TiO_2 can only be excited by UV light due to its wide band gap energy (3.2 eV for anatase), which is not ideal to absorb visible light [7–9]. One of the most efficient ways to improve photocatalytic activity of TiO_2 is the generation of defects in the lattice through selective metal or nonmetal ion doping because it can lead to a lower band gap, and thus improve the sunlight utilization of TiO_2 [10, 11]. Additionally, the recombination of electron–hole pairs is suppressed by doping of TiO_2 with other elements. But, the main point is that the double elements co-doped TiO_2, such as Ag and Pd [12], Cu and Zn [13], Ni and Ag [14], Cu and S [15], Ag and I [16], N and C [17], Co and Fe [18], and F and N [19], apparently display higher photocatalytic activity than mono-doped TiO_2, and some of the above-mentioned elements have synergistic effects on the photocatalytic reactions. Riaz et al. [20] demonstrated that Cu and Ni co-doped TiO_2 powders prepared via precipitation method showed a higher photocatalytic activity in the degradation of Orange II under visible light as compared to monometallic and undoped TiO_2. Ryo and his colleagues synthesized (Ni, Ta or Ni, Nb) co-doped TiO_2 photocatalysts that showed higher visible light absorption intensity and higher water splitting activity than that of the pure TiO_2 under visible

light irradiation [21]. Various methods used for doping of TiO_2 involve ion implantation, sol–gel reaction, hydrothermal reaction, solid-state reaction, etc. [11, 22–24], of which the sol–gel process is absolutely very simple. It controls the size and shape of the nanoparticles and does not require any special equipment. Expanding on this line of research, we attempted to prepare novel photocatalytic materials by the sol–gel method to explore the synergism induced by Ag and Mg co-doped TiO_2 nanoparticles, because compared to transition metals and rare earth metals, doping with alkaline earth metals such as Mg and Ca have rarely been reported to-date.

Hence, the present paper deals with the synthesis of TiO_2, Ag/TiO_2, Mg/TiO_2 and bimetallic Ag, Mg/TiO_2 nanoparticles using the sol–gel method. The catalytic activity of bimetallic Ag, Mg/TiO_2 catalyst was compared with its corresponding monometallic Ag/TiO_2, Mg/TiO_2, and TiO_2 catalysts in the degradation of C.I. Acid Red 27 (AR27) from the aqueous solution under visible light. The structural properties of the prepared photocatalysts were further characterized using X-ray diffraction (XRD), scanning electron microscopy (SEM), energy dispersive X-ray spectroscopy (EDX), transmission electron microscopy (TEM), UV–Vis diffuse reflectance spectroscopy (DRS), X-ray photoelectron spectroscopy (XPS), photoluminescence (PL), and specific surface area and porosity analysis (BET and BJH).

Experimental design

Materials

Magnesium nitrate hexahydrate and silver nitrate were used as dopant metal salts. Titanium tetraisopropoxide ($Ti(OC_3H_7)_4$) was used as the titania precursor. Methanol (MeOH) was of 95 % purity and AR27 was used as the model azo dye for photocatalytic degradation study. All compounds were obtained from Merck Chemical Company, Germany.

Synthesis of TiO_2 and doped TiO_2 nanoparticles using sol–gel method

Pure TiO_2, single-doped, and Ag, Mg co-doped TiO_2 nanoparticles were successfully prepared by the sol–gel method using titanium isopropoxide (TTIP) as the titania precursor. For co-doped TiO_2 sample, first TTIP, methanol and distilled water were maintained in a molar ratio of 1:1:65. TTIP was mixed with methanol and sonicated for 5 min. To this solution, distilled water was added dropwise under vigorous stirring and reflux conditions at 80 °C for 3 h; then appropriate amounts of $Mg(NO_3)_2$ and $AgNO_3$ dissolved in water were added to the mixed solution and the obtained solution was stirred for 1 h. The resulting transparent colloidal suspension was dried and finally calcined at 450 °C for 3 h. Monometallic and pure TiO_2 were also prepared by the same procedure (Fig. 1).

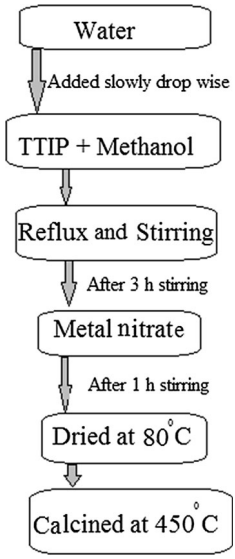

Fig. 1 Schematic diagram of the sol–gel method for the preparation of the catalysts

Characterization methods

XRD patterns for phase identification and crystallite size calculation were recorded with a Siemens D5000 X-ray diffraction using Cu Kα radiation (recorded in the $2\theta = 20°–70°$). The average crystallite size (D in nm) was calculated using Scherrer's equation (Eq. 6) [25]:

$$D = k\lambda/\beta \cos\theta \tag{6}$$

where k is a constant equal to 0.89, λ is the X-ray wavelength equal to 0.154056 nm, β is the full width at half maximum intensity (FWHM), and θ is the half diffraction angle.

The DRS of the samples was obtained using Avaspec-2048 TEC spectrometer to determine the optical band gap (E_g) of the catalysts. The band gap energies of all samples were calculated by the following equation (Eq. 7):

$$E_g\,(\text{eV}) = 1240/\lambda\,(\text{nm}) \tag{7}$$

TEM observation was carried out on Philips CM-10 HT—100 keV electron microscopy instrument. The chemical composition of the prepared catalysts was analyzed by an EDX system. SEM analysis was performed on Au-coated samples using a Philips apparatus model XL30. Nitrogen adsorption–desorption was carried out using Belsorp mini II instrument to measure the specific surface area. The mean pore diameter and total pore volume of the co-doped sample were measured using the Brunauer–Emmett–Teller (BET) and the Barret–Joyner–Halender (BJH) methods. Photoluminescence emission spectra of the samples were recorded using a JASCO luminescence spectrometer with excitation wavelength of 320 nm. The

surface chemical composition of samples was analyzed by XPS (XPS, twin anode XR3E2 X-ray source).

Photocatalytic activity of the catalysts

Photocatalytic degradation of 20 mg L^{-1} AR27 was conducted using halogen lamp 500 W (Osram) as a visible light source. In the experiment, 40 mg of photocatalyst was added to 100 mL of distilled water and sonicated for 15 min in an ultrasonic bath at 25 °C, followed by addition of AR27 to give rise to a final concentration of 20 mg L^{-1} and volume of 100 mL. Prior to irradiation, the suspension containing the catalyst was stirred using a magnetic stirrer for 30 min in the dark to ensure the establishment of adsorption–desorption equilibrium of AR27 on the catalyst surface. After 30 min, this suspension was illuminated for 30 min using a 500 W halogen lamp. During the irradiation experiments, 5 mL of the sample was taken out at certain time intervals, centrifuged for 30 min to remove the suspended solid photocatalyst, and analyzed with a UV–Vis spectrophotometer (UV-Shimadzu 2100).

Results and discussion

XRD analysis

The crystalline phase of undoped and doped TiO_2 with Ag and Mg calcined at 450 °C for 3 h was analyzed. Figure 2 shows XRD patterns of Ag/TiO_2 (0.08 mol%), Mg/TiO_2 (0.2 mol%), and Ag, Mg/TiO_2 (0.08–0.2 mol%) calcined at 450 °C. The peaks at 25.4°, 37.8° and 48° explain the diffractions of the (101), (004) and (200) anatase-type TiO_2, which can be indexed as the anatase phase of TiO_2, whereas XRD peaks at 27.4° (110) and 55° belong to the rutile form. The average crystallite sizes are calculated according to the Debye–Scherrer equation. The average crystalline size of all the samples is about 20 nm. For all the samples, no obvious changes on their crystallite size and crystal structure were observed after Ag and Mg doping. It can be concluded that the major phase of these samples is anatase phase and trace amounts of rutile exist. The XRD patterns didn't show any metal phase, indicating that Ag and Mg are uniformly dispersed among the anatase crystallites, which might be due to the small amount of dopants or their high dispersion in the samples [26].

TEM analysis

The size, shape, and distribution of Ag, Mg/TiO_2 nanoparticles can be clearly observed in the TEM image (Fig. 3). The micrograph of the photocatalyst shows that the formed nanoparticles were homogeneous with no significant phase separations on the surface. The size of the Ag, Mg/TiO_2 nanoparticles corresponds to the crystallite size calculated by the XRD patterns.

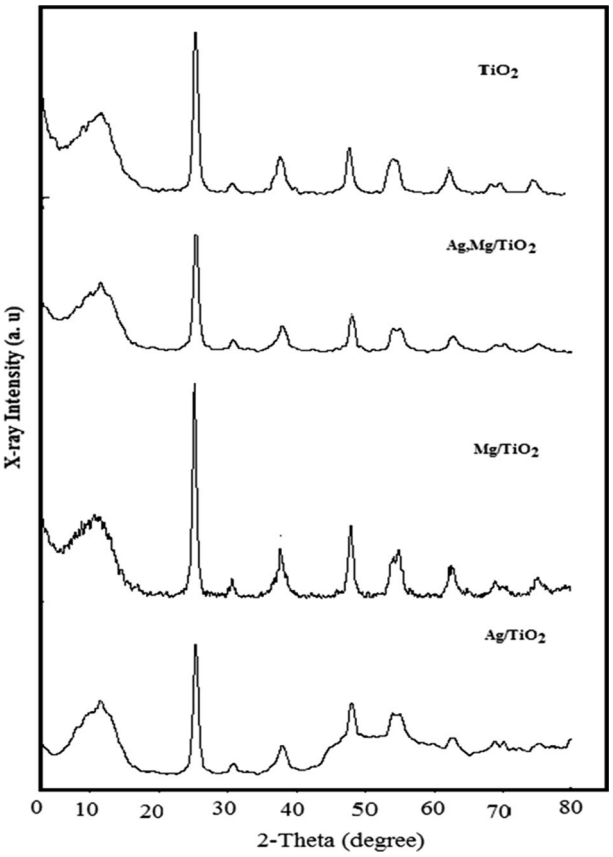

Fig. 2 XRD patterns of TiO_2, Ag/TiO_2 (0.08 mol%), Mg/TiO_2 (0.2 mol%) and Ag, Mg/TiO_2 (0.08–0.2 mol%) calcined at 450 °C

SEM analysis

The structural characterization of doped TiO_2 nanoparticles was carried out via SEM. Figure 4 shows the SEM micrograph of the Ag and Mg co-doped TiO_2 calcined at 450 °C, which indicates a dense structure with fairly good homogeneity. There is a uniform distribution of agglomerated particles. This image shows the particles with a spherical morphology.

EDX and mapping analysis

The EDX used to identify elements exists in the prepared catalyst. The EDX analysis (Fig. 5a) showed that Ti, O, Ag, and Mg peaks were obviously found in the spectra, confirming the presence of both Ag and Mg in the co-doped TiO_2. The Mapping spectrum (Fig. 5b) of the photocatalysts showed that the dopant metals were well dispersed on the TiO_2. These findings are consistent with the XRD results, indicating that the doped metals were well dispersed on the TiO_2 surface.

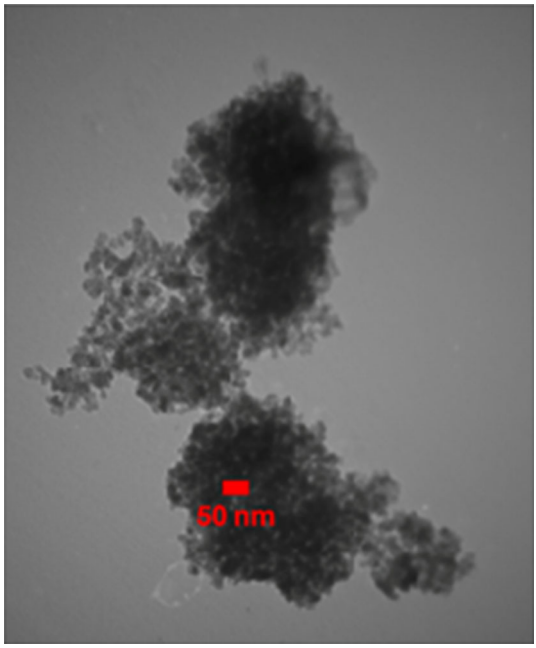

Fig. 3 TEM image of Ag, Mg/TiO_2 calcined at 450 °C

BET and BJH analysis

The plot of N_2 adsorption–desorption isotherm and the BJH pore size distribution plot of the representative samples are given in Fig. 6. The specific surface areas measured for Ag/TiO_2, Mg/TiO_2, and Ag, Mg/TiO_2 were 75.6, 65.8, and 85.9 $m^2\ g^{-1}$, respectively. The pore size distribution of the Ag, Mg/TiO_2 nanoparticles was obtained from adsorption branch, using the BJH method in the range of 10.18 nm. The BET surface area results indicated that there is a significant increase in the surface area of co-doped catalyst. Higher specific surface areas can improve the adsorption ability of photocatalysts, because the photocatalytic activity strongly depends on better adsorption of organic substrate and the interfacial charge transfer can also be enhanced [27].

DRS analysis

The DRS of the TiO_2, Mg/TiO_2, Ag/TiO_2, and Ag, Mg/TiO_2 nanoparticle samples are given in Fig. 7. The absorption spectrum of TiO_2 consists of a single broad intense absorption around 400 nm due to the charge transfer from the valence band to the conduction band. The band gap energies of all samples are shown in Table 1. This reduction of band gap may be attributed to the doping of Ag and Mg^{2+} as impurity on the TiO_2 surface and production of extra energy within the band gap [28]. The results indicated that Ag and Mg co-doped onto TiO_2 decreased the optical band gap energy, whereas the decrease in Eg value for Ag, Mg/TiO_2 is

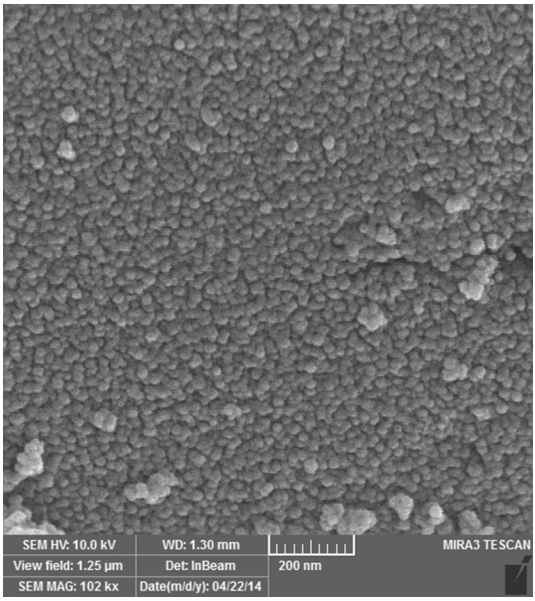

Fig. 4 SEM of Ag, Mg/TiO_2 calcined at 450 °C

greater than that for monometallic catalysts. The co-doped TiO_2 with Mg and Ag showed a considerable shift in the absorption peak towards the visible region. The tailing absorption peaks can be considered as the extra tail states in the band gap because of the synergistic effect of added Mg and Ag to the TiO_2 surface. The extension of absorption edge to longer wavelengths for Ag, Mg/TiO_2 shows the presence of good contact between TiO_2 and Mg and Ag particles and enhances the photocatalytic activity of catalysts in the visible light.

XPS analysis

The XPS survey spectrum of Ag, Mg/TiO_2 indicates that the peak contains Ti, Ag, Mg and O atoms. The survey spectrum and high resolution scans are shown in Fig. 8. It can be seen that the Ag 3*d* XPS spectrum consist of two major peaks at 367.07, 373.09 eV, corresponding to Ag $3d_{5/2}$ and Ag $3d_{3/2}$ binding energies, respectively, and the spin energy separation is 6.0 eV, indicating that Ag species exist in their metallic state [29]. The binding energy of Mg 2*p* was found to be 50.21 eV, which is typical of Mg^{2+} [30]. The binding energies of Ti $2p_{3/2}$ and Ti $2p_{1/2}$ were found to be 458.21 and 464.015 eV and these bands indicate that the Ti element mainly exists as the chemical state of Ti^{4+} [31].

PL analysis

Figure 9 shows the PL spectra of the pure TiO_2, mono-doped, and co-doped TiO_2 nanoparticles excited by 320 nm. The PL emission in semiconductors arises from the recombination of free electron–hole; therefore, the PL spectra were used to study the transfer, migration, and recombination processes of the photogenerated

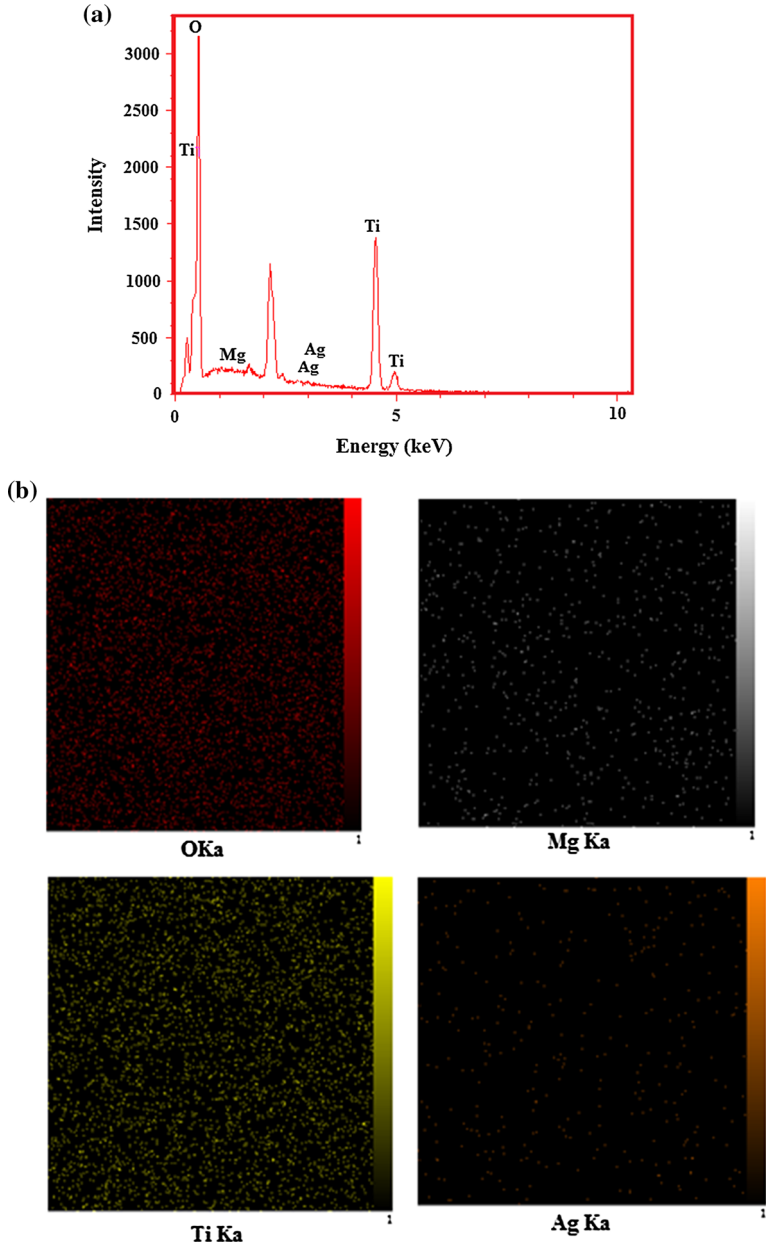

Fig. 5 **a** EDX spectrum of Ag, Mg/TiO_2 nanoparticles, **b** mapping spectrum of Ag, Mg/TiO_2 nanoparticles

electron–hole pairs [32]. As is discernible from this figure, there is a considerable decrease in the intensity of PL spectra of co-doped TiO_2 compared to that of the pure and mono-doped TiO_2. The lower intensity of the peak suggests that the Mg

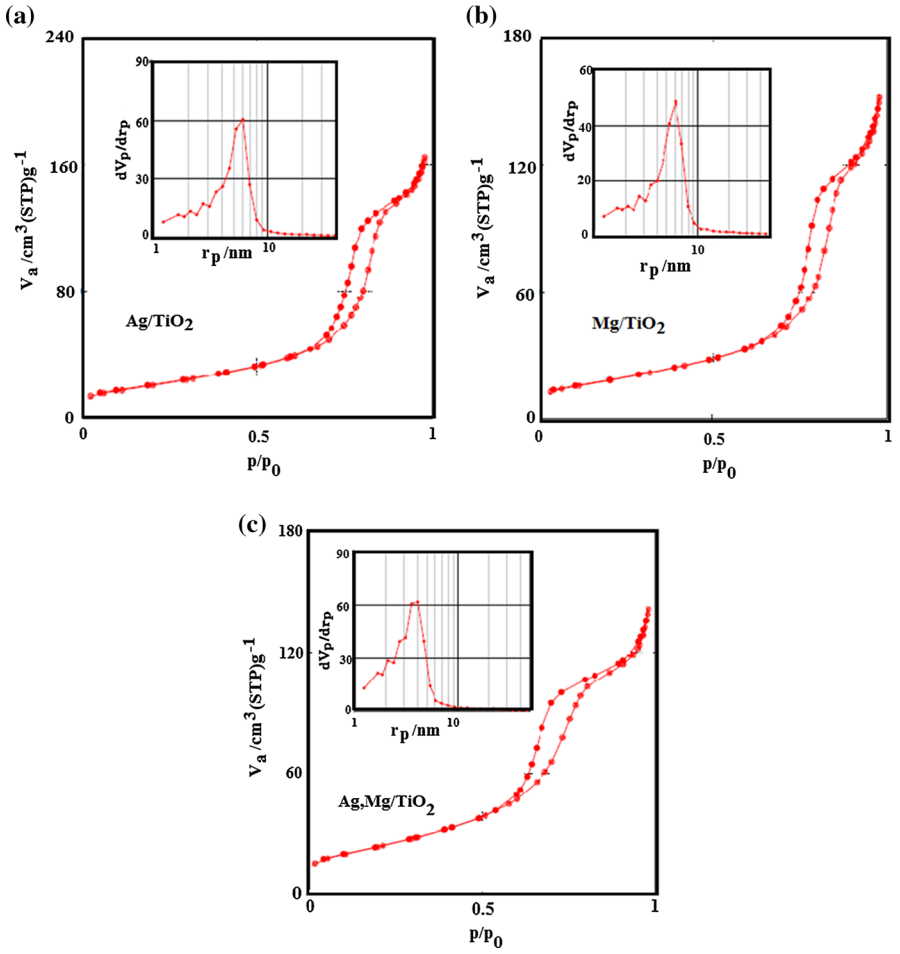

Fig. 6 N_2 adsorption–desorption isotherm of the Ag/TiO_2 (0.08 mol%), Mg/TiO_2 (0.2 mol%) and Ag, Mg/TiO_2 (0.08–0.2 mol%) nanoparticles calcined at 450 °C

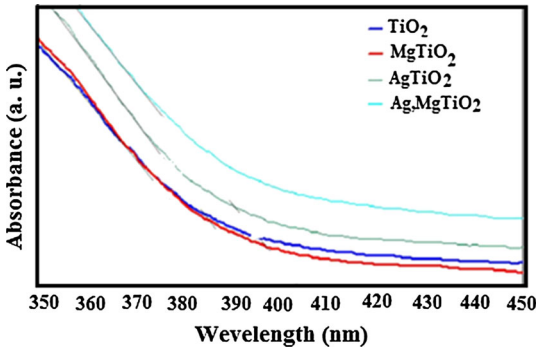

Fig. 7 The DRS–UV–Vis spectra of TiO_2, Mg/TiO_2, Ag/TiO_2 and Ag, Mg/TiO_2 nanoparticles

Table 1 E_g values for monometallic and bimetallic silver and magnesium doped TiO_2 nanoparticles

Catalyst	λ_{max} (nm)	E_g (eV)
TiO_2	392	3.61
Ag/TiO_2	396	3.31
Mg/TiO_2	392	3.61
$Ag, Mg/TiO_2$	404	3.07

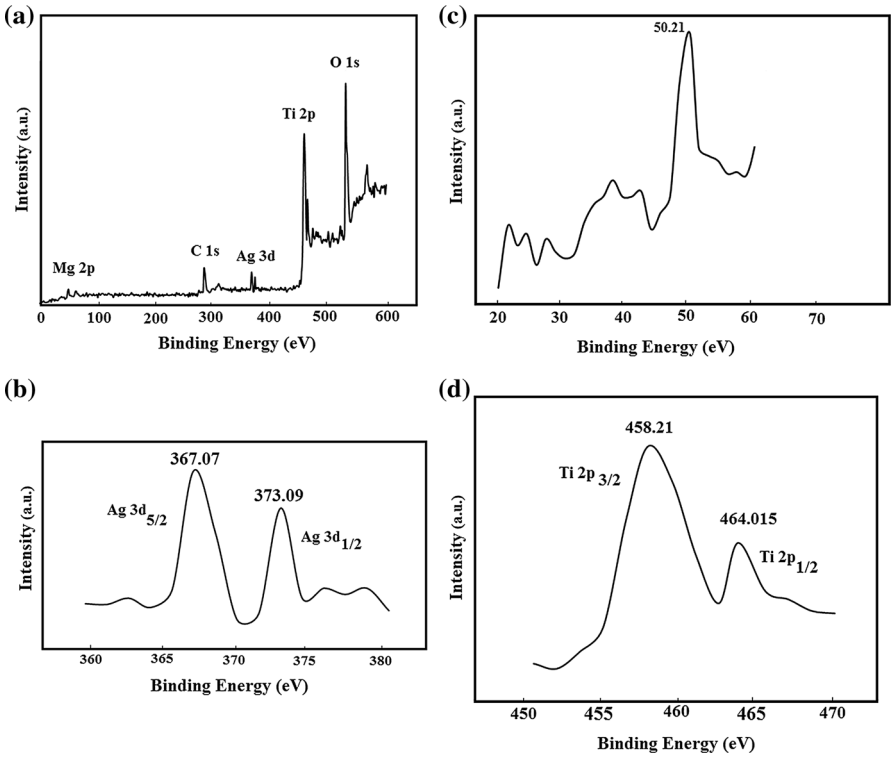

Fig. 8 **a** XPS survey spectrum of magnesium and silver co-doped TiO_2, **b** High resolution of Ag 3*d* spectrum, **c** high resolution of Mg 2*p*, **d** high resolution of Ti 2*p* spectrum

and Ag co-doped on the surface of TiO_2 could effectively inhibit the recombination probability of photogenerated electrons and holes, due to the separate charge transfer between the Ag, Mg and TiO_2 [33] (Fig. 9).

Photocatalytic performance

The semi-logarithmic graph of the concentration of AR27 in the presence of various photocatalysts versus visible light irradiation time yields straight lines, which confirms the pseudo-first order kinetics for the removal of AR27 in this process. The

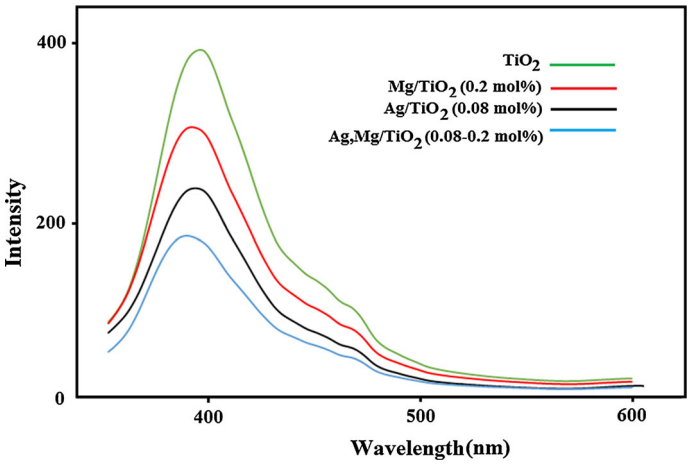

Fig. 9 PL spectra of pure TiO_2, Ag/TiO_2 (0.08 mol%), Mg/TiO_2 (0.2 mol%) and Ag, Mg/TiO_2 (0.08–0.2 mol%) nanoparticles

apparent reaction rate constant (k_{ap}) for photocatalytic removal of AR27 was obtained from the slope of the semi-logarithmic graphs [34]. Table 2 summarizes all the obtained k_{ap} for the removal of AR27 in the presence of various catalysts under different calcination temperatures. According to these results, k_{ap} increased with Ag loading up to 0.08 mol%. In the photocatalytic process, metallic Ag, which acts as a sink for photo-induced charge carriers, can promote interfacial charge transfer processes and prevent the recombination of photogenerated electron–hole pairs due to its strong electron trap ability, and thus increase the photocatalytic activity. Further increasing the silver content above 0.08 mol% decreased the photocatalytic activity due to screening the TiO_2 surface from light absorption and reducing the active sites on the nanocatalyst. According to the k_{ap} results in Table 2, for Mg doped TiO_2 nanoparticles, the highest photocatalytic activity was obtained at Mg content of 0.2 mol%. This may be attributed to the fact that increased dopant concentration leads to increased number of trapped charge carriers per particle, extending the lifetime of the photogenerated electron–hole pairs. However, an excessive Mg content at the surface of TiO_2 acts as a significant recombination center for photogenerated electron–hole pairs, and prevents the interfacial electron–hole to transfer, leading to decreased photoactivity [35]. The results shown in Fig. 10 and Table 2 show that bimetallic Ag, Mg/TiO_2 photocatalyst containing 0.08 mol% Ag and 0.2 mol% Mg has better photocatalytic activity than Ag/TiO_2, Mg/TiO_2, and pure TiO_2, because silver and magnesium can separately trap photogenerated electrons and inhibit electron–hole recombination and consequently improve photocatalytic activity. Furthermore, another factor for enhancing the photocatalytic performance of the co-doped catalyst is its large surface area.

These results confirm previous studies that reported enhanced photoactivity for the bimetallic Cu–Ni/TiO_2 photocatalyst by Gao et al. [36], Nurlaela et al. [37], Riaz et al. [38, 39]. The co-doping technique also improves the physical properties

Table 2 The apparent reaction rate constant (k_{ap}) for different catalysts in the photocatalytic degradation of AR27

Catalyst	Metal doping (mol%)		Calcination temp (°C)	k_{ap} (min^{-1})
	Ag	Mg		
TiO_2	0	0	450	0.0480
Mg/TiO_2	0	0.2	450	0.0557
Ag/TiO_2	0.02	0	450	0.0498
Ag/TiO_2	0.05	0	450	0.0543
Ag/TiO_2	0.08	0	450	0.0712
Ag/TiO_2	1	0	450	0.0672
Ag, Mg/TiO_2	0.08	0.15	450	0.0741
Ag, Mg/TiO_2	0.08	0.2	450	0.1219
Ag, Mg/TiO_2	0.08	0.5	450	0.0981
Ag, Mg/TiO_2	0.08	1	450	0.0713
Ag, Mg/TiO_2	0.08	0.2	400	0.0871
Ag, Mg/TiO_2	0.08	0.2	550	0.0751
Ag, Mg/TiO_2	0.08	0.2	650	0.0498

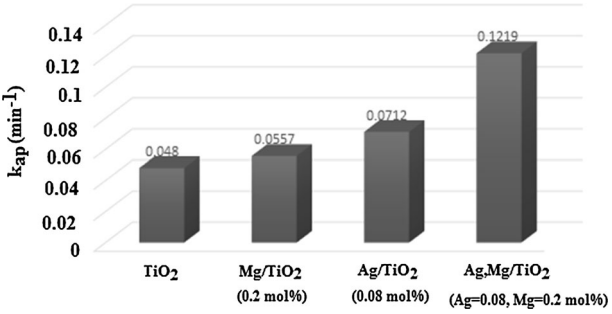

Fig. 10 Comparison between the photocatalytic activity of TiO_2, Mg/TiO_2, Ag/TiO_2 and Ag, Mg/TiO_2 nanoparticles in the removal of AR27 under visible light irradiation

of the TiO_2, such as specific surface area and crystallite size, while it sustains the phase transformation of anatase to rutile phase [40]. In order to study the influence of the calcination temperature on the photocatalytic activity of the catalyst, the Ag (0.08 mol%) and Mg (0.2 mol%) were calcined at 400, 450, 550, and 650 °C for 3 h. As shown in Fig. 11, calcination temperature, which could reach a maximum of 450 °C, has important effect on the photocatalytic activity of co-doped TiO_2 nanoparticles. Calcination process can influence the surface area, morphology, and crystallinity of the prepared photocatalyst. When temperature was lower than 450 °C, samples still contained more amorphous TiO_2, which was not useful for producing the above-mentioned e^- and h^+, and therefore the catalytic activity decreased. With increasing temperature, the transformation from amorphous to

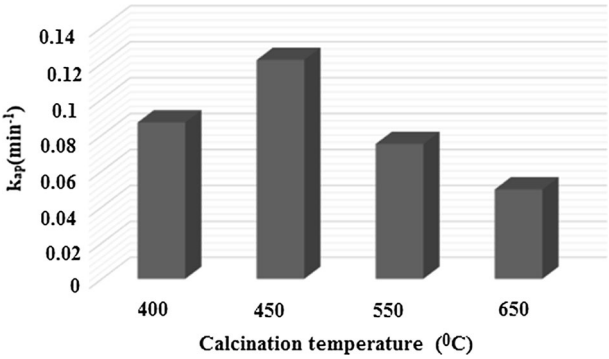

Fig. 11 Effect of calcination temperature on photocatalytic activity of Ag, Mg/TiO_2 nanoparticles in the removal of AR27 under visible light irradiation

anatase increased, while anatase TiO_2 had higher photocatalytic activity; consequently, photocatalytic activity gradually increased. However, when calcination temperature was above 450 °C, TiO_2 could change from anatase to rutile and particle size would increase with increasing the temperature. Its internal porosity and specific surface were reduced, recombination rate between e^- and h^+ was increased; therefore, the catalytic activity was reduced [41].

Conclusion

Pure TiO_2, single-doped, and Ag, Mg co-doped TiO_2 nanoparticles were successfully prepared by the sol–gel method. The XRD patterns of the photocatalysts did not show the presence of separate metal diffraction peaks for Ag or Mg phases. This is mainly due to the high dispersion of the Ag and Mg on TiO_2. DRS results indicated a considerable decrease in Eg value for Ag, Mg/TiO_2 nanoparticles in comparison with bare and monometallic doped TiO_2 nanoparticles. The BET results showed an increase in the surface area of the catalyst, which increased the photocatalytic degradation of AR27 in visible light. TiO_2 co-doped with 0.08 mol% Ag and 0.2 mol% Mg exhibited the highest photocatalytic activity in the photocatalytic degradation of AR27, compared to monometallic and undoped TiO_2. Enhanced photodegradation of AR27 using Ag, Mg/TiO_2 photocatalyst clearly indicated the prevention of electron–hole recombination, which is one of the major limitations of TiO_2. Such an activity was attributed to the synergistic effects of Ag and Mg co-doping TiO_2. The optimum calcination temperature was 450 °C.

Acknowledgments The authors would like to gratefully acknowledge the support of Islamic Azad University, North Tehran Branch.

References

1. D.M. Blake, *National Renewal Energy Laboratory*, (Golden, CO, USA, 2001)

2. H.K. Singh, M. Saquib, M.M. Haque, M. Muneer, J. Hazard. Mater. **142**, 374–380 (2007)
3. U.G. Akpan, B.H. Hameed, J. Hazard. Mater. **170**, 520–529 (2009)
4. O. Legrini, E. Oliveros, A.M. Braun, J. Chem. Rev. **93**, 671 (1993)
5. T. Sugimoto, X. Zhou, A. Muramatsu, J. Colloid Interface Sci. **259**, 43 (2003)
6. M.A. Behnajady, H. Eskandarloo, Chem. Eng. J. **228**, 1207–1213 (2013)
7. M. Muruganandham, N. Sobanaa, M. Swaminathan, J. Hazard. Mater. **137**, 1371–1376 (2006)
8. W. Liu, S. Chen, W. Zhao, S. Zhang, Desalination **249**, 1288–1293 (2009)
9. J. Mills, J. Wang, Photochem. Photobiol. **127**, 123–134 (1999)
10. T.C. Dang, D.L. Pham, H.C. Le, V.H. Pham, J. Nanosci. Nanotechnol. **01**, 5002 (2010)
11. X. Chen, S.S. Mao, J. Chem. Rev. **107**, 2891–2959 (2007)
12. K. Kontapakdee, J. Panpranot, P. Praserthdam, Catal. Commun. **8**, 2166–2170 (2007)
13. D. Zhang, F. Zeng, J. Phys. Chem. A **85**, 1077–1083 (2011)
14. H.Y. Chuang, D.H. Chen, J. Nanotechnol. **20**, 105704 (2009)
15. M. Hamadanian, A. Reisi-Vanani, A. Majedi, J. Appl. Surf. Sci. **256**, 1837 (2010)
16. L. Liao, C.W. Ingram, J. Appl. Catal. A **433**, 18–25 (2012)
17. K.R. Wu, C.W. Yeh, C.H. Hung, C.Y. Chung, L.H. Cheng, J. Nanosci. Nanotechnol. **10**, 1057 (2010)
18. W. Zhuyi, C. Chen, F. Wu, B. Zou, M. Zhao, J. Wang, C. Feng, J. Hazard. Mater. **2**, 615–620 (2009)
19. G. Yang, T. Wang, B. Yang, Z. Yan, S. Ding, Appl. Surf. Sci. **287**, 135–142 (2013)
20. N. Riaza, F.K. Chongb, B.K. Duttac, Z.B. Mana, M.S. Khana, E. Nurlaelaa, Chem. Eng. J. **185**, 108–119 (2012)
21. R. Niishiro, H. Kato, A. Kudo, Phys. Chem. Chem. Phys. **7**, 2241–2245 (2005)
22. U.G. Akpan, B.H. Hameed, J. Appl. Catal. A **375**, 1–11 (2010)
23. E.D. Jeong, P.H. Borse, J.S. Jang, J.S. Lee, O.S. Jung, H. Chang, J.S. Jin, M.S. Won, H.G. Kim, J. Ceram. Process Res. **9**, 250–253 (2008)
24. D.H. Kim, S.I. Woo, S.H. Moon, H.D. Kim, B.Y. Kim, J.H. Cho, Y.G. Joh, E.C. Kim, J. Solid State Chem. **136**, 554–558 (2005)
25. A.L. Patterson, J. Phys. Rev. **56**, 978–982 (1939)
26. Y. Li, S. Peng, F. Jiang, G. Lu, S. Li, J. Serb. Chem. Soc. **72**, 393–402 (2007)
27. H. Shi, T. Zhang, T. An, B. Li, X. Wang, J. Colloid Interface Sci. **380**, 121–127 (2012)
28. Q. Wang, S. Xu, F. Shen, Appl. Surf. Sci. **257**, 7671–7677 (2011)
29. L. Sun, J. Li, C. Wang, S. Li, Y. Lai, H. Chen, C. Lin, J. Hazard. Mater. **171**, 1045–1050 (2009)
30. J.S. Corneille, J. Wei He, D. Wayne Goodman, Surf. Sci. **306**, 269–278 (1994)
31. S.S. Mandal, A.J. Bhattacharyya, J. Chem. Sci. **124**, 969–978 (2012)
32. J. Ren, W. Wang, S. Sun, L. Zhang, J. Chang, Appl. Catal. B **92**, 50–55 (2009)
33. Y.M. Wu, H.B. Liu, J.L. Zhang, F. Chen, J. Phys. Chem. C **113**, 14689–14695 (2009)
34. M.A. Behnajady, N. Modirshahla, R. Hamzavi, J. Hazard. Mater. **133**, 226–232 (2006)
35. S. Ahmed, M.G. Rasul, W.N. Martens, R. Brown, M.A. Hashib, Desalination **261**, 3–18 (2010)
36. W. Gao, R. Jin, J. Chen, X. Guan, H. Zeng, F. Zhang, N. Guan, Catal. Today **90**, 331–336 (2004)
37. E. Nurlaela, F.K. Chong, B.K. Dutta, N. Riaz, in *International Conference on Fundamental and Applied Sciences (ICFAS2010)*, (2010), pp. 15–17
38. N. Riaz, F.K. Chong, B.K. Dutta, M.S. Khan, E. Nurlaela, in *International Conference on Fundamental and Applied Sciences (ICFAS2010)*, (Convention Centre, Kuala Lumpur, 2010)
39. N. Riaz, F.K. Chong, B.K. Dutta, M.S. Khan, E. Nurlaela, in *2nd International Conference on Environmental Science and Technology, IPCBEE*, (2011), pp. 111–117
40. C. Wen, Y.J. Zhu, T. Kanbara, H.Z. Zhu, C.F. Xiao, Desalination **2**, 621–625 (2009)
41. M.A. Behnajady, H. Eskandarloo, J. Nanosci. Nanotechnol. **13**(1), 548–553 (2013)